Early proteasome downregulation and dysfunction drive proteostasis failure in Alzheimer's disease

Shan Jiang,[1,2,†] Malavika Srikanth,[1,2,†] Rossana Serpe,[1,2] Shadi Yavari,[1,2] Pallavi Gaur,[2,3] Galen Andrew Collins,[4] Rajesh Soni,[1,5] Vilas Menon[2,3] and Natura Myeku[1,2]

[†]**These authors contributed equally to this work.**

Abstract

Alzheimer's disease (AD) is characterized by the accumulation of pathogenic proteins, notably amyloid-beta and hyperphosphorylated tau, which disrupt neuronal function and contribute to cognitive decline. Although proteotoxic stress is well-established in AD, the role of the ubiquitin-proteasome system (UPS) in maintaining neuronal proteostasis, and how it becomes compromised during disease progression remains incompletely understood.

Here we integrated multiple approaches to characterize proteasome function, composition, and regulation in post-mortem human AD brain tissue compared to age-matched controls. These included proteasome kinetic assays, affinity purification of intact 26S proteasomes, in-gel activity assays and proteomics. According to Braak staging, we further interrogated bulk RNA-seq and single-nucleus RNA-seq (sn-RNA-seq) datasets spanning the progression of AD pathology. Finally, we examined Nrf1/NFE2L1 binding and subcellular localization to understand the transcriptional regulation of proteasome genes in AD.

We found that proteasome activity is significantly impaired in AD brains, affecting both 26S and 20S complexes. This reduction in proteolytic capacity persisted after proteasome purification, implicating intrinsic defects within the proteasome complex. Proteomic profiling of isolated proteasomes revealed diminished abundances of constitutive proteasome complexes and the co-purification of proteasomes with aggregation-prone substrates (e.g., tau, α-synuclein and SQSTM1/p62), suggesting proteasome entrapment in pathological aggregates. Transcriptomic analyses showed progressive downregulation of constitutive proteasome subunit genes in individuals along the Braak stage axis, with downregulation apparent even at the earliest Braak

stages, in tissue without overt tau aggregation. Neurons were disproportionately affected, whereas non-neuronal cells did not show substantial differences in proteasome-related gene expression, possibly through immunoproteasome induction. Despite elevated NFE2L1 expression, a key transcription factor normally driving proteasome gene transcription, AD brains exhibited impaired Nrf1 nuclear localization, preventing the expected compensatory upregulation of proteasome components.

Collectively, our findings suggest that proteasome dysfunction in AD arises early and deepens over the disease course. Intrinsic alterations in proteasome complexes, coupled with early transcriptional downregulation of proteasome subunits and disrupted Nrf1-mediated regulatory pathways, contribute to a vicious cycle of proteotoxic stress and neuronal vulnerability. Restoring proteasome function and enhancing Nrf1-driven transcriptional responses may represent promising therapeutic strategies to preserve proteostasis and mitigate neurodegeneration in AD.

Author affiliations:

1 Department of Pathology and Cell Biology, Columbia University Irving Medical Center. New York, NY, USA

2 The Taub Institute for Research on Alzheimer's Disease and the Aging Brain, Columbia University Irving Medical Center. New York, NY, USA

3 Department of Neurology, Columbia University Irving Medical Center. New York, NY, USA

4 Department of Biochemistry, Nutrition, and Health Promotion, Mississippi State University, Mississippi State, MS, USA

5 Proteomics and Macromolecular Crystallography Shared Resource, Herbert Irving Comprehensive Cancer Center, Columbia University, New York, NY, USA

Correspondence to: Natura Myeku

Columbia University Irving Medical Center

The Taub Institute for Research on Alzheimer's Disease and the Aging Brain

630 W 168th St. P&S Building Room 12-403

New York, NY, 10032, USA

E-mail: nm2631@cumc.columbia.edu

Running title: Early proteasome downregulation in AD

Keywords: Alzheimer's disease; tau aggregation; proteostasis; proteasome; Nrf1 (NFE2L1); RNA-sequencing

Introduction

AD is a progressive neurodegenerative disorder characterized by the pathological accumulation of two hallmark proteins: amyloid-beta (Aβ) and tau. These aggregates manifest prominently in regions critical for cognition and memory, such as the hippocampus and neocortex, eventually disrupting neuronal communication, inducing synaptic loss, and leading to widespread neurodegeneration and dementia[1]. Less frequently highlighted is the fact that ubiquitin is a major component of these intracellular aggregates[2], suggesting that dysregulated ubiquitin–proteasome-mediated degradation may be either a downstream result of disease pathogenesis or an active contributor to it.

The UPS selectively degrades regulatory, short-lived and misfolded proteins through ubiquitin tagging and subsequent proteolysis by the 26S proteasome[3-5]. This ATP-dependent, ~2.5 MDa macromolecular machinery consists of a 20S core particle (CP) harboring proteolytic sites, capped by one or two 19S regulatory particles (RP) that recognize, unfold, and translocate substrates into the CP[6]. The proteasome clears damaged proteins and modulates regulatory protein abundance, thereby critically maintaining neuronal proteostasis and survival.

Proteasome activity declines with aging[7], rendering post-mitotic neurons particularly vulnerable to toxic protein accumulation, especially in proteotoxic conditions such as AD. Reduced proteasome function may represent an early event tipping the balance toward pathogenic protein accumulation. Proteasome biogenesis is regulated transcriptionally by the transcription factor NFE2L1 (Nrf1), which binds antioxidant response elements (AREs) in promoters of proteasome

subunits and assembly chaperones[8-10]. Nrf1 initially anchors to the endoplasmic reticulum (ER) membrane and, under normal conditions, is rapidly degraded via ER-associated degradation (ERAD)[8,11]. Nrf1 is firstly ubiquitinated by the ER-bound HRD1 (E3 ligase) followed by retro-translocation to the cytoplasm by p97/VCP where it is immediately degraded by the proteasome (half-life ~12 min). However, when proteasome capacity is diminished, cytoplasmic Nrf1 (>120kDa) is stabilized and undergoes de-glycosylation and truncation by NGLY1 (an N-glycanase) and the DDI2 protease, respectively to generate a transcriptionally active Nrf1 (<120kDA) which is then translocated to the nucleus to bind to the ARE promoter region present in all proteasome genes to induce de novo proteasomes. This "proteasome bounce-back" response is an evolutionarily conserved mechanism that ensures rapid upregulation of proteasome genes when degradation capacity is compromised[12]. Despite this adaptive bounce-back response, in AD, this compensatory mechanism may become ineffective, contributing to the accumulation of toxic proteins.

Historically, proteasomes were considered passive peptidases rather than critical regulators of the UPS and protein homeostasis[2]. However, recent work from our group[13-16] and others[17-22] have highlighted the proteasome as a fundamental regulator whose dysfunction could significantly influence protein aggregation in neurodegenerative diseases.

In the present study, we aimed to clarify proteasome dysfunction in AD by characterizing the functional, proteomic, and transcriptomic state of proteasomes in post-mortem human AD brains compared to cognitively normal controls. Using affinity purification, kinetic assays, in-gel activity assays, and proteomics, along with bulk and single-nucleus RNA-seq analyses, we investigated how proteasome composition and function correlate with AD severity. Our findings revealed reduced substrate degradation and decreased proteasome complexes in AD brains. Furthermore, proteasomes co-purified with aggregating proteins, including tau, α-synuclein, and p62, suggesting that proteasomes are not only functionally impaired but also physically trapped within pathological protein aggregates.

By analyzing multiple bulk RNA-seq and snRNA-seq datasets across Braak stages, we identified an early and pronounced downregulation of constitutive proteasome subunit genes. This transcriptional decline preceded substantial tau aggregation and worsened as pathology advanced. Around Braak stage IV, we observed the emergence of immunoproteasome components, an

inducible proteasome subtype typically expressed by non-neuronal cells during inflammation[23,24]. This finding suggests compensatory proteasome expression by glial cells in response to the inflammatory environment characteristic of AD[25], coinciding with neuronal loss of intrinsic proteasomal capacity.

To investigate the mechanisms underlying reduced proteasome gene expression, we examined Nrf1, a master regulator of proteasome transcription[8,10]. Subcellular fractionation demonstrated diminished nuclear Nrf1 and elevated cytosolic Nrf1 in AD brains, indicating impaired nuclear translocation. This accumulation of Nrf1 in the cytoplasm reduces its availability for transcriptional activation of proteasome genes, further exacerbating proteasomal deficits.

Collectively, our data reveal a consistent and early reduction in proteasome gene expression in AD, likely contributing to impaired proteasome function, and facilitating the buildup of aggregation-prone proteins. As pathogenic proteins accumulate, they may further inhibit proteasome activity, creating a detrimental feedback loop that amplifies neuronal dysfunction and progressive neurodegeneration. The transcriptional downregulation of Nrf1 signaling identified here provides critical insight into the molecular events underlying proteostasis collapse in AD. Our results underscore potential therapeutic opportunities aimed at enhancing proteasome activity, improving Nrf1-mediated transcriptional responses, or intervening to prevent early proteasome subunit downregulation.

Materials and methods

Further methodological details are provided in the Supplementary Materials

Human Post-Mortem Brain Tissues

Human post-mortem brain tissue samples were obtained from the New York Brain Bank at Columbia University Irving Medical Center (CUIMC). Complete demographic details of the cases included in this study are provided in **Supplementary Table 1**. Specimens were snap-frozen and stored at −80°C. Cases (Control, n=40; AD Braak V/VI, n=60) underwent neuropathological characterization to assign Braak stages and were subsequently separated into grey and white matter for region-specific analyses.

Cell lines

We utilized HEK293-derived clonal cell lines (DS1 and DS9), originally generated by Dr. Marc Diamond's laboratory[26], which stably express the repeat domain of 2N4R tau bearing the P301L and V337M disease-associated mutations fused to YFP (RD-P301L/V337M-YFP).

Native In-Gel Proteasome Activity Assay

Cortical samples (~50–100 mg) were homogenized in buffer (50 mM Tris-HCl, 5 mM $MgCl_2$, 5 mM ATP, protease/phosphatase inhibitors), centrifuged at 20,000 × g, and protein concentrations measured by Bradford assay. Equal protein amounts underwent native PAGE at 160 V for 180 min (4°C). Proteasome activity was visualized with 100 µM Suc-LLVY-amc (G1101, UBP Bio) under UV transillumination and quantified via ImageJ.

Affinity Purification of 26S Proteasomes

Frozen cortical tissues (~500 mg) were homogenized and centrifuged (100,000 × g, 30 min, 4°C). Soluble fractions were incubated with recombinant GST-UBL and glutathione–Sepharose resin (17075601, Cytiva) for proteasome capture. Proteasomes were eluted using recombinant His-UIM and purified via Ni^2+-NTA agarose (Qiagen). Particle concentration was estimated assuming 2.5 MDa per proteasome.

Proteasome Kinetics Assay

Purified proteasomes (15 nM) were incubated with 50 µM Suc-LLVY-amc substrate. Fluorescence (380/460 nm) was measured at 2–5 min intervals over 120 min using a TECAN Spark reader. Initial reaction velocity was calculated from linear fluorescence increases.

Western Blot Analysis and Subcellular Fractionation

Tissues (~50 mg) or cells were lysed in RIPA buffer, sonicated, and centrifuged (3,000 × g, 10 min, 4°C). Protein concentrations (BCA assay) were adjusted to 1 µg/µL in LDS sample buffer. Proteins (20 µg/sample) were separated via NuPAGE 4–12% Bis-Tris gels, transferred to nitrocellulose membranes, blocked (5% milk/TBST), and incubated overnight with primary antibodies: Nrf1 (1:1000), PSMG1 (1:1000), PSMC3 (1:2500), Lamin A/C (1:4000), GAPDH (1:8000), β-Actin (1:8000) (Cell Signaling Technologies; Enzo Life Sciences). HRP-conjugated secondary antibodies were used, and chemiluminescent signals were quantified by ImageJ.

Subcellular Fractionation

Nuclear and cytoplasmic fractions were isolated from tissues/cells using NE-PER reagents (Thermo Fisher). Fractions were validated by Western blotting for Lamin A/C (nuclear) and GAPDH (cytosolic).

Quantitative Proteomics

Proteins from gel-isolated or affinity-purified 26S proteasomes underwent denaturation (0.5% sodium deoxycholate, 100 mM Tris-HCl, pH 8.5), reduction/alkylation (TCEP/CAA), and overnight trypsin/LysC digestion. Acidified peptides were desalted with SDB-RPS StageTips, dried, and resuspended (3% acetonitrile, 0.1% formic acid). PASEF-based LC-MS/MS analysis utilized a timsTOF Pro 2 mass spectrometer. Peptides were separated on a C18 column (IonOpticks) over a 65-minute gradient (300 nL/min flow, 0.1% formic acid in water/acetonitrile). Ion mobility (1/K0=0.6–1.4 V·s/cm²) and mass (m/z 100–1700) ranges were set; collision energy was 59 eV.

LC-MS/MS Data Analyses

Raw data were processed with MaxQuant (v.2.4.10.0) against UniProt human proteome. Trypsin specificity allowed two missed cleavages; cysteine carbamidomethylation was fixed, and acetylation, oxidation, phosphorylation, and GlyGly modifications were variable. Peptide/protein identifications were at 1% FDR, with LFQ quantification for differential abundance analyses using DEP in R. Missing values were imputed; differential proteins (FDR<0.05) were visualized via volcano plots and heatmaps. Protein-protein interaction (PPI) networks were constructed using STRING database interactions visualized by igraph in R.

Bulk RNA-Seq Data Analysis

Bulk RNA-seq data from MSBB, ROSMAP, and Mayo cohorts (AD Knowledge Portal) underwent variance-stabilizing normalization (DESeq2). Multivariate ordinal regression related normalized expression to Braak stages, adjusting for covariates (RIN, age, sex, PMI, etc.) with FDR correction. Gene-level heatmaps (pheatmap) and proteasome complex expression bar plots were generated from Z-score–normalized values. Meta-analysis (R package meta) assessed proteasome expression differences between AD and controls.

snRNA-seq Data Analysis

SnRNA-seq datasets from DLPFC ROSMAP employed pseudo-bulking by cell type, normalized via DESeq2. Multivariate ordinal regression related expression to Braak stage, adjusting for covariates with FDR correction. Circular heatmaps visualized complex-level proteasome gene expression per cell type and Braak stage.

NFE2L1 ChIP-seq Data Analysis

NFE2L1 ChIP-seq data from HepG2 cells (ENCODE) assessed proteasome promoter binding using ChIP peak Anno in R. Proteasome gene binding was compared against background genes via random sampling (10,000 iterations); distributions analyzed using Student's t-test (two-tailed).

NFE2L1 Resist Score

To quantify NFE2L1's impact on proteasome expression, linear regression modeled normalized NFE2L1 versus proteasome 26S expression. An Nrf1 resist score (NRS = predicted - observed proteasome expression) quantified deviations from expected proteasome transcriptional activation. Scores indicated samples where proteasome transcription was impaired (positive NRS) or compensatory mechanisms existed (negative NRS).

Statistical analyses

Statistical analyses for Figures 1 and 7 were performed using GraphPad Prism 10 (GraphPad Software, San Diego, CA). Normality was tested by the D'Agostino-Pearson or Shapiro-Wilk tests. Variance homogeneity was assessed using Levene's test. Proteasome kinetics assays of total lysates (**Fig. 1B, D**) and native in-gel proteasome activity assays from gray matter (**Fig. 1J**) were analyzed by Mann-Whitney tests. Kinetics assays of purified proteasomes (**Fig. 1F, H**) and in-gel proteasome assays from white matter (**Fig. 1L**) were evaluated using two-tailed unpaired Student's t-tests. Immunoblot data for Nrf1 (**Fig. 7B**) used the Mann-Whitney test, whereas PSMG1 and Rpt5 (**Fig. 7C, D**) analyses employed two-tailed unpaired Student's t-tests. Immunoblots from subcellular fractions (**Fig. 7I–K**) utilized two-way ANOVAs with Bonferroni corrections. Statistical significance is indicated as follows: *P < 0.05, **P < 0.01, ***P < 0.001, ****P < 0.0001, ns = not significant.

Statistical Analyses for Bioinformatics Data

Bioinformatics analyses were conducted in R. Significance was set at two-tailed $P < 0.05$ unless specified. False discovery rate (FDR) corrections accounted for multiple testing.

Proteomics Analyses

Raw proteomics data were processed using the R package DEP. Proteins not consistently identified across replicates in at least one group (control or AD) were excluded. Bar plots display identified proteins per sample (**Supplementary Figures 1A, 3A, 5A, 7A**). Variance-stabilizing normalization (VSN) was performed, visualized by box plots before and after normalization (**Supplementary Figures 1B, 3B, 5B, 7B**). Missing data were imputed using the MinProb distribution method, and smoothed density curves assessed imputation effectiveness (**Supplementary Figures 1C, 3C, 5C, 7C**). Principal component analysis (PCA) was applied to the 50 most variably expressed proteins to visualize data structure and potential batch effects (**Supplementary Figures 1D, 3D, 5D, 7D**). Differential abundance was determined via empirical Bayes statistics, controlling for FDR at $P < 0.05$.

Bulk RNA-Seq Analyses

Proteasome gene and complex-level expression across Braak stages were analyzed from three AD cohorts: MSBB, ROSMAP, and Mayo Clinic. Multivariate ordinal regression models were fitted:

For **MSBB**, the regression model, *Braak score ~ gene/complex expression + RNA integrity number (RIN) + sex + ethnicity + age + post-mortem interval (PMI) + library size*, was used. For **ROSMAP**, the regression model, *Braak score ~ gene/complex expression + RIN + sex + ethnicity + education + age + PMI + library size*, was used.

For the **Mayo Clinic**, the regression model, *Braak score ~ gene/complex expression + RIN + sex + age + library size*, was used. Since all Mayo samples were from a white population, ethnicity was not included in this model. In these models, library size is an intermediate variable introduced by DESeq2 for normalization. FDR correction was used for multiple testing, and significance was assessed at $p < 0.05$. FDR corrections were applied ($P < 0.05$). Meta-analysis across these cohorts used standardized mean differences (AD_{mean} - $Control_{mean}$) pooled with a fixed-effect model using the R package meta (**Fig. 4G**) and significance determined at $P < 0.05$.

snRNA-seq Analyses

Cell-type–specific proteasome gene expression was assessed using pseudo-bulking to avoid single-nucleus analytical biases. For each sample and each cell type c, we aggregated all nucleus-level read counts for each gene g:

For a given cell type in a given sample, pseudo-bulking for each gene was performed with the formula $E_{g,c} = \sum_{i=1}^{n_c} E_{g,c,i}$, where $E_{g,c}$ is the single nucleus sequencing read count for gene g across all the nuclei of a certain cell type c, n_c is the total cell count in the cell type c, and $E_{g,c,i}$ is the read count for gene g in the ith cell of the cell type c.

After pseudo-bulking for all the genes in individual samples for a certain cell type, we obtained a gene-by-sample read count matrix $M_{g\times s}$ for the cell type.

The resulting pseudo-bulk data were variance-stabilizing normalized (VSN) in *DESeq2*, and we fit multivariate ordinal regression models similar to those above to relate proteasome subunit gene expression to the Braak stage for each cell type. The multivariate ordinal regression model was: *Braak score ~ gene expression + RIN + sex + ethnicity + education + age + PMI + library size*, was used. The false discovery rate (FDR) approach was applied to multiple testing corrections. $P < 0.05$ was considered significant.

NFE2L1 ChIP-Seq Enrichment and Statistical Comparison

NFE2L1 (Nrf1) promoter occupancy for proteasome genes was compared against randomly selected background genes. Stratified random sampling (10,000 peak-signal samples per group) was performed from NFE2L1 ChIP-seq data. Peak intensity distributions were compared using an unpaired, two-tailed Student's t-test (equal variance). Normality was confirmed by the Kolmogorov–Smirnov test ($P < 0.05$).

NFE2L1 Resist Score (NRS)

To quantify the extent of proteasome recovery through *NFE2L1* by leveraging transcriptomics, we computed the *NFE2L1* resist score (NRS) as the difference between the predicted proteasome expression by a linear regression model and the observed proteasome expression. To compute the predicted proteasome expression, the model function fit by the linear regression with the expression of *NFE2L1* as the explanatory variable and the expression of the proteasome as the

response variable was used: $\hat{y} = \beta x + \varepsilon$, where $\hat{y}$ is the predicted proteasome expression, x is the *NFE2L1* expression, β is the coefficient and ε is a random variable representing the noise. Then the *NFE2L1* resist score was calculated with the formula NRS = $\hat{y}$ - y, where y is the observed proteasome expression. The three cohorts (parahippocampal gyrus from MSBB, ROSMAP and prefrontal cortex from Mayo study) were combined to compute NRS. The dataset batch effect was removed. To investigate the effect of tau aggregation on NRS, a multivariate linear regression model with the formula, $NRS \sim Braak\ Score + RIN + sex + ethnicity + age + PMI$, was used. $P < 0.05$ was considered significant.

Results

Impaired Degradation Capacity of Proteasomes from AD Brains

A central feature of AD and other neurodegenerative disorders is the disruption of cellular proteostasis, an imbalance between protein synthesis, folding, and degradation leading to the accumulation of misfolded and aggregated proteins[27,28]. The UPS, with the 26S proteasome at its core, plays a pivotal role in maintaining neuronal proteostasis by selectively degrading aberrant or damaged proteins[3-5]. Despite its recognized importance, the precise regulation, functionality, and regional specificity of the proteasome in AD remain underexplored. While previous studies have reported reduced proteasome activity in AD-affected brain regions[29,20,30], these studies relied mostly on endpoint assays using total tissue lysates, potentially capturing non-specific activities. To address these limitations, we employed three complementary assays to assess proteasome function specifically in Brodmann area 9 (BA9), a region heavily implicated in dementia[31,32]. We separated post-mortem human brains into grey matter (neuronal somata-rich) and white matter (primarily glial and axonal structures), allowing investigation of proteasome activity across distinct cellular contexts[33].

Using kinetic fluorogenic substrate digestion over a two-hour period, proteasomes from both grey and white matter extracts in AD brains displayed a significantly reduced rate of substrate hydrolysis compared to non-cognitively impaired controls (**Fig. 1A-D**). These results suggest a widespread impairment of proteasome-mediated proteolysis in AD brains.

To ensure that these deficits were not merely reflective of altered proteasome abundance as opposed to the activity or the presence of additional proteases in crude lysates, we next purified 26S proteasomes from brain tissue using an affinity chromatography–based assay adapted from Besche and Goldberg[34], which is a well-established method in our lab[13]. Under standardized conditions with equal proteasome concentrations (~15nM), purified AD-derived 26S proteasomes showed substantially decreased degradative activity relative to controls (**Fig. 1E-H**). This confirms intrinsic functional deficits within the proteasome complex, independent of cellular milieu influences. Additionally, native in-gel activity assays[35] which preserve 26S and 20S proteasome conformations, revealed marked reductions in both 26S and 20S proteasome activities in grey matter from AD brains (**Fig. 1I,J**). In white matter, 26S proteasome activity similarly declined, whereas the decrease in 20S proteasome activity did not reach statistical significance (**Fig. 1K,L**). These observations suggest differential susceptibility of proteasome subtypes (26S vs. 20S) in a region- and cell-type-specific manner, reflecting distinct proteostatic demands across neuronal and glial populations. Supporting this, purified proteasome assays that specifically measure functional 26S complexes without interference from 20S or non-specific proteases showed the greatest inhibition (~50–70%).

Collectively, these results demonstrate that proteasomes from AD brains exhibit reduced degradative capacity, reflecting intrinsic structural changes within the proteasome itself as well as extrinsic alterations in the AD cellular environment, contributing to impaired proteostasis in AD.

Proteasome Complexes are Reduced in AD Brains

Having demonstrated compromised proteasome activity in AD brains, we next evaluated how proteasome abundance and composition are altered. We isolated 26S proteasome-containing gel bands from in-gel activity assays and conducted high-resolution proteomics (PASEF-based) from grey and white matter samples of non-cognitively impaired (control, n=12) and AD (n=14) brains to assess regional proteasome differences associated with AD pathology. Quantitative proteomics identified and quantified 655 proteins in grey matter, encompassing all known proteasome subunits: alpha (PSMA1–7), beta (PSMB1–10) subunits of the 20S core, and ATPase (PSMC1–6) and non-ATPase (PSMD1–14) subunits of the 19S regulatory particle[36]. Differential analysis

identified 359 significantly altered proteins (189 decreased, 170 increased) in AD relative to controls (**Fig. 2A**). Constitutive 26S proteasome subunits were markedly decreased in AD (**Fig. 2B**), indicating that reduced proteolytic activity (Fig. 1E–H) likely results not only from functional impairments but also from lower proteasome complex abundance. Elevated levels of aggregation-prone proteins, tau (MAPT) and α-synuclein (SNCA), were also observed, implicating proteasome deficiency in pathological protein accumulation (**Fig. 2A**). Consistent with this, our earlier studies showed purified proteasomes exposed to tau aggregates or oligomers exhibit reduced proteolytic activity[13], providing mechanistic evidence for aggregate-driven proteasome impairment.

A comparative heatmap of proteasome subunits alongside ubiquitin-mediated proteolysis factors (E3 ligases, DUBs, molecular chaperones) demonstrated selective downregulation of the 19S, 20S, and immunoproteasome subunits in AD, rather than a global UPS suppression (**Fig. 2C**). Protein–protein interaction (PPI) networks further validated these findings: proteasome subunits in grey matter were consistently reduced along with critical proteostasis regulators, including E3 ubiquitin ligases (CUL1, CUL3, HUWE1, SKP1), chaperones (CCT complex members, HSP90AB1, STIP1, BAG3), and the proteasome stabilizer ECM29 (**Fig. 2D** and **Supplementary Fig. 2**). Conversely, tau, α-synuclein, molecular chaperones (HSPA1A/HSP70, HSPA8/HSC70, TRAP1, HSPD1/HSP60), and ubiquitin shuttles/DUBs (UBC, RAD23B, UBQLN2, USP14, NPLOC4) were elevated, reflecting compensatory responses to disrupted proteostasis (**Fig. 2D and Supplementary Fig. 2**). Although these alterations likely reflect disease-stage proteostatic adjustments, the persistent loss of core proteasome subunits points to a compromised final degradation step.

In white matter, we quantified 456 proteins, including all proteasome subunits, yet found only 55 proteins significantly altered (**Fig. 2E**). Unlike grey matter, proteasome subunits did not exhibit significant reductions (**Fig. 2F,G**). The white matter PPI network showed decreased E3 ligases (CUL1, CUL3) and select chaperones (HSP90AB1, CCT2, CCT3), but increased levels of HSP70 family chaperones (HSPA1A, HSPA8, HSPA4, HSPA5, HSPA9, HSPD1) and STIP1, suggesting an adaptive response (**Fig. 2H and Supplementary Fig. 4**).

We next analyzed affinity-purified intact 26S proteasomes from grey and white matter using similar quantitative proteomics approaches. In grey matter, we quantified 1200 proteins, revealing 52 significantly altered (22 decreased, 30 increased) in AD relative to controls (**Fig. 3A**). Although

reductions of 26S proteasome subunits were not statistically significant in this purified fraction, their consistent downward trend supports the reduced mature proteasome complexes observed in AD brains (**Fig. 3B**), aligning with the observed decline in proteolytic activity. A heatmap analysis showed no global UPS alterations, further emphasizing the selective vulnerability of the proteasome complex itself (**Fig. 3C**).

The PPI network analysis of grey matter affinity-purified samples revealed a dense cluster of reduced proteasome subunits alongside decreased levels of key proteostasis factors, including E3 ligases (CUL1, HUWE1), COP9 signalosome components (COPS2–6, GPS1), chaperones (HSP90AB1, CCT2, CCT3, HSPA5), and critical regulators of Nrf1 signaling (VCP, DDI2) (**Fig. 3D** and **Supplementary Fig. 6**). Additionally, UPS adaptors and DUBs (ECM29, PSMF1, UBQLN1/2, USP14, NPLOC4) were reduced. Conversely, AD-linked aggregation-prone substrates tau and α-synuclein, stress-associated chaperones (HSPA1A, HSPA4, HSPA9), and the proteotoxic marker SQSTM1/p62 were enriched, indicating proteasome sequestration by pathogenic aggregates (**Fig. 3D** and **Supplementary Fig. 6**).

For affinity-purified white matter proteasomes, we identified 693 proteins, of which 78 were significantly altered (43 decreased, 35 increased; **Fig. 3E**). However, proteasome subunits showed no marked or statistically significant reductions (**Fig. 3F**). A heatmap of UPS factors revealed only subtle, heterogeneous alterations (**Fig. 3G**). PPI network analysis indicated a balanced state with decreased levels of chaperones (CCT2, CCT3, HSPA9, HSP90, STIP1) and ubiquitin adaptors (UBC, UBEA, USP14, UBX1) contrasted by increases in E3 ligases (CUL1, CUL3, HUWE1, SKP1), COP9 signalosome components (COPS2–6, GPS1), chaperones (HSPA8, HSPD1, HSPA4, HSPA1), and proteostasis-related factors (tau, PSMF1, RAD23B) (**Fig. 3H and Supplementary Fig. 8**). Thus, white matter maintains a relatively intact proteasome composition despite proteostatic stress.

In summary, our findings reveal pronounced regional differences in proteostasis dysregulation in AD. Grey matter demonstrates substantial depletion of proteasome complexes and associated proteostasis factors, coupled with accumulation of aggregation-prone proteins. Conversely, white matter retains relatively stable proteasome levels with moderate proteostasis alterations. These regional differences highlight grey matter's heightened vulnerability in AD pathology progression.

Comprehensive protein quantifications and supporting data are provided in supplementary materials and tables.

Constitutive proteasome genes are decreased with the progression of Braak stages in AD

Our findings thus far indicate that proteasome function is diminished at both the enzymatic activity and proteomic levels in AD. To further investigate whether these impairments are reflected at the transcriptional level and to clarify how proteasome subunit gene expression relates to AD progression, we first examined bulk RNA-seq datasets from three large, well-characterized cohorts: the Mount Sinai Brain Bank (MSBB) with 299 brain samples from multiples regions[37], the Religious Orders Study and Memory and Aging Project (ROSMAP) with 633 brain samples[32] and the Mayo Clinic Study of Aging with 319 brain samples[38]. Together, these datasets encompass 1251 samples of the full spectrum of AD pathology, as indexed by Braak staging[31]. Multivariate ordinal regression models adjusted for confounders confirmed that observed transcriptional changes were independent of age, sex, education, ethnicity, and postmortem interval.

Heatmaps revealed pronounced and progressive downregulation of constitutive proteasome subunits including 19S regulatory (PSMC, PSMD) and 20S core particles (PSMA, PSMB) starting at early Braak stages and intensifying with disease progression across all cohorts (**Fig. 4A–C**). Assembly chaperones (PSMG1–4), essential for proteasome maturation and stability[36], mirrored this decline (**Fig. 4A–C**). Within the MSBB cohort, this transcriptional pattern appeared consistently across multiple cortical regions, notably the parahippocampal gyrus (PHG), a region prominently affected early in AD (**Fig. 4A and Supplementary Fig. 9A–C).** Interestingly, the cerebellum from the Mayo cohort did not show similar reductions (**Supplementary Fig. 9D**), indicating regional specificity of these changes.

For quantitative assessment, we aggregated proteasome genes by functional complexes (19S, 20S, assembly chaperones, immunoproteasome (IP), and IP activators) and plotted Z-scores against Braak stages (**Fig. 4D–F**). Both MSBB and ROSMAP consistently showed significant decreases in 19S and 20S proteasome complex gene expression correlating with disease progression (**Fig.**

4D,E; Supplementary Fig. 9E–G). The Mayo dataset, though more variable, supported this general trend (**Fig. 4F; Supplementary Fig. 9H**). Thus, constitutive proteasome impairment begins early, preceding extensive tau aggregation, and worsens with advancing pathology.

In contrast, immunoproteasome components exhibited distinct expression profiles, showing stability or slight increases around Braak stage IV when constitutive proteasomes sharply decline (**Fig. 4A–F; Supplementary Fig. 9**). Immunoproteasomes, induced under oxidative stress and inflammation conditions prevalent in AD[39], likely represent an adaptive response to increasing proteotoxicity and neuroinflammation. Although potentially beneficial in clearing damaged proteins, enhanced immunoproteasome activity may inadvertently exacerbate inflammation.

A fixed-effect meta-analysis integrating data across the three cohorts provided robust confirmation, revealing significant negative standardized mean differences for 19S, 20S complexes, and assembly chaperones (**Fig. 4G**). Immunoproteasome subunits, however, showed smaller, less consistent changes, underscoring their unique regulatory dynamics in AD pathology (**Fig. 4G**).

Collectively, our results demonstrate a reproducible, progressive reduction in constitutive proteasome subunit expression early in AD, correlating tightly with tau pathology. This transcriptional decline, observed consistently across multiple cohorts and regions, emphasizes proteostasis failure's central role in AD pathogenesis. These data highlight the potential therapeutic importance of interventions aiming to restore proteasome function or mitigate its early dysfunction in AD.

snRNA-Seq Analyses Reveal Neuron-Specific Proteasome Reductions

To further dissect the cell-type–specific alterations in proteasome expression identified in our bulk RNA-seq analyses, we examined two recently published snRNA-seq datasets (Fujita et al.[40] and Mathys et al.[41]) from dorsolateral prefrontal cortex (DLPFC) tissue samples from 619 non-overlapping brains, totaling over 3.9 million single nuclei and spanning a range of Braak stages in AD (**Fig. 5**). Building on the patterns previously observed where bulk RNA-seq analyses suggested

a pronounced and progressive decline in constitutive proteasome subunits (**Fig. 4**), snRNA-seq data from ROSMAP studies reveal a neuron-specific decrease in proteasome gene expression (**Fig. 5**). These two independent datasets provide a complementary, high-resolution view of proteasome dysregulation across multiple brain cell types and across AD pathology.

In both the Fujita et al.[40] (**Fig. 5A**) and Mathys et al.[41] (**Fig. 5B**) datasets, concentric circular heatmaps visualize proteasome-related gene expression (19S, 20S, assembly chaperones, IP, and IP activator complexes) as a function of Braak stages, with each ring segment representing a distinct cell type and each radial segment denoting a proteasome complex class. Across increasing Braak stages, excitatory and inhibitory neurons consistently exhibit a substantial reduction in the expression of constitutive proteasome complexes and their assembly chaperones (**Fig. 5**). This neuron-specific decline aligns closely with our earlier findings from the bulk-tissue analyses of ROSMAP and other two datasets. Here extra information suggests that neurons are particularly vulnerable to proteostatic stress in AD (**Fig. 5**). In fact, our findings align well with recently published data demonstrating that induced pluripotent stem cell (iPSC)-derived neurons from 53 individuals in the ROSMAP cohort show reduced expression of proteasome components specifically in excitatory neurons derived from AD patients[42].

In contrast, non-neuronal cells, including astrocytes, microglia, oligodendrocytes, and endothelial cells do not follow this neuronal pattern. Their proteasome-related gene expression remains stable or even increases for certain components, particularly the immunoproteasome and its activators PA28αβ and PA28γ (PSME1-3) (**Fig. 5**). This indicates that non-neuronal cells either maintain proteasome function or mount adaptive responses against proteotoxic stress. Such differential resilience could explain the relative resistance of non-neuronal cells to pathological protein aggregation, consistent with our earlier proteomic observations in white matter.

Collectively, these results reinforce our findings of proteasome impairment predominantly affecting neurons, aligning with bulk RNA-seq meta-analyses across multiple independent cohorts. The consistency of these observations in distinct snRNA-seq datasets from Fujita et al[40]. and Mathys et al.[41] strongly supports neuronal proteasome insufficiency as a key contributor to accumulating neurotoxic proteins and subsequent proteostasis collapse characterizing AD progression. Moreover, the contrasting responses in non-neuronal cell types, exhibiting stable or elevated proteasome levels, underscore the cell-type-specific vulnerability and compensatory

mechanisms during disease progression. These data highlight proteasome dysfunction not merely as an artifact of dataset-specific biases, but rather as a robust, fundamental hallmark of AD pathology, particularly pronounced in vulnerable neuronal populations.

Elevated NFE2L1 Expression Fails To Sustain Proteasomes, Uncovering Regulatory Collapse In AD

To further elucidate the molecular mechanisms underlying the progressive downregulation of proteasome transcripts in AD brains, we turned our attention to NFE2L1/Nrf1, a master transcription factor responsible for the coordinated regulation of all proteasome subunits[8,10]. Utilizing publicly available NFE2L1 ChIP-seq data from human cell lines generated by the ENCODE Project Consortium[43], we found significant enrichment of NFE2L1 binding at loci encoding proteasome subunits compared to random background genes (**Fig. 6A**; $p=9.8\times10^{4}$, two-sample Kolmogorov–Smirnov test). This confirms NFE2L1's direct involvement in regulating proteasome genes as part of the cellular "proteasome bounce-back" response when proteolytic capacity is challenged.

We then assessed whether the transcriptional decline in proteasome subunits in AD correlated with changes in NFE2L1 expression using bulk RNA-seq data across three independent cohorts spanning early-to-late Braak stages. Surprisingly, despite the progressive reduction in proteasome subunit expression, NFE2L1 and the related transcription factor NFE2L2/Nrf2 which activates proteasome genes during oxidative stress[44,45] exhibited increased expression in advanced Braak stages (**Fig. 6B**). This apparent paradox suggests that increased transcription factor levels fail to maintain proteasome transcription, possibly due to impaired NFE2L1 activation, nuclear translocation, or altered signaling dynamics.

To quantify the functional relationship between NFE2L1 expression and proteasome abundance, we developed an "NFE2L1 resist score," derived from linear regression modeling. This score represents deviations between the actual proteasome 26S (P26S) content and levels predicted by NFE2L1 expression alone (**Fig. 6C**). Scores near zero reflect normal NFE2L1-proteasome coupling, negative scores indicate higher-than-expected proteasome content (potentially adaptive

responses), and positive scores indicate impaired proteasome production despite sufficient transcriptional signals from NFE2L1.

Analyzing resist scores across Braak stages, we found early-stage (Braak 0) samples had negative scores, reflecting robust proteasome abundance with low NFE2L1 levels (**Fig. 6D**). However, with advancing pathology (Braak VI), scores became significantly positive ($p=9.88\times10^{7}$), revealing that higher NFE2L1 transcription did not translate into corresponding increases in proteasome abundance. This indicates a breakdown in the NFE2L1-mediated transcription-to-proteasome assembly pathway in advanced AD.

Collectively, these findings highlight a critical regulatory failure: despite elevated transcription factors designed to upregulate proteasome genes under proteostatic stress, the expected proteasome induction does not occur. This implies progressive dysfunction within the Nrf1 activation cascade, particularly ER-to-nucleus signaling required for effective proteasome gene expression. Understanding and restoring this regulatory pathway may prove essential for re-establishing neuronal proteostasis and reducing pathology in AD.

Nrf1 Stabilization and Impaired Proteasome "Bounce-Back" Response in AD Brains

To evaluate the transcriptional regulatory potential of Nrf1 in AD, we examined its protein levels and subcellular localization in proteasome-enriched cortical (BA9) extracts. Western blot analysis revealed significantly increased total Nrf1 protein (upper and lower bands) in AD compared to control samples (**Fig. 7A,B**), whereas levels of the proteasome assembly chaperone PSMG1 were notably reduced (**Fig. 7A,C**). The 19S proteasome subunit Rpt5/PSMC3 showed a trend toward reduction that was not statistically significant (**Fig. 7A,D**).

The increased Nrf1 in AD brains likely results from impaired proteasome-mediated degradation, reflecting diminished proteolytic activity. Normally, active proteasomes maintain low Nrf1 levels by rapid turnover; however, reduced proteasome function stabilizes Nrf1, activating a compensatory "bounce-back" mechanism designed to restore proteasome abundance.

Surprisingly, despite elevated Nrf1 protein, AD brains do not exhibit the anticipated increase in proteasome subunits, highlighting an impaired compensatory response.

Subcellular fractionation further illuminated Nrf1 dysregulation. Immunoblotting showed significantly elevated cytosolic Nrf1 and reduced nuclear Nrf1 in AD compared to controls (**Fig. 7E–G**). This indicates that Nrf1 accumulates in the cytosol but fails to translocate effectively into the nucleus, thus limiting its transcriptional activation of proteasome genes. Proper fractionation was confirmed using Lamin A/C (nuclear marker) and GAPDH/β-actin (cytosolic controls) (**Fig. 7E**).

Overall, our findings suggest a stalled Nrf1-driven proteasome bounce-back mechanism in AD, characterized by cytoplasmic Nrf1 accumulation and impaired nuclear localization, ultimately contributing to insufficient proteasome transcriptional responses.

Cellular Models Confirm Nrf1-Mediated Proteasome Bounce-Back Response Under Proteasome Impairment

To further investigate how reduced or inhibited proteasome activity affects the bounce-back response, we examined two cell lines, DS1 and DS9 clones generated from HEK 293 cells[26] which both express truncated disease associated mutant tau but differ in their proteostasis status. DS1 cells, lacking tau aggregates, represent intact proteostasis, while DS9 cells, with persistent tau aggregation, model compromised proteasome function. Accordingly, western blot analyses revealed that DS9 cells show significantly increased Nrf1 forms in the total, cytosolic and nuclear fraction compared to DS1 cells (**Fig. 7 H,I**), consistent with reduced proteasome-mediated degradation. Following overnight treatment with the proteasome inhibitor epoxomicin (50 nM), both cell lines exhibited significantly stabilized Nrf1 in total, cytosolic, and nuclear fractions showing a complete inhibition of Nrf1 degradation by the proteasome under epoxomicin conditions (**Fig. 7H,I**). Concomitantly, elevated levels of the proteasome assembly chaperone PSMG1 and the 19S subunit Rpt5/PSMC3 were detected in non-treated condition in DS9 cells when proteasome activity was reduced (**Fig. 7H,J,K**). And under epoxomicin treatment, when proteasome activity was inhibited (**Fig. 7H,J,K**), confirming the activation of the expected

compensatory response- Nrf1 stabilization, nuclear translocation, and proteasome subunit upregulation in response to proteasome impairment. Complete nuclear accumulation of Nrf1 after epoxomicin exposure affirmed that proteasome inhibition robustly triggers Nrf1 translocation, activating downstream proteasome gene expression (**Fig. 7H,I**). Proper fractionation was verified using nuclear (Lamin A/C) and cytosolic (GAPDH, β-actin) markers (**Fig. 7H**).

Our findings reveal that while Nrf1 stabilization and nuclear localization effectively mediate proteasome bounce-back responses in cellular models, this pathway is disrupted in AD brains, highlighting a crucial disconnect between transcriptional activation and effective proteasome recovery, thereby exacerbating proteostatic collapse in AD.

Discussion

Our findings provide an integrated view of proteasome insufficiency in AD, encompassing transcriptional deficits, reduced enzymatic activity, and impaired compensatory responses. Given the correlative nature of postmortem studies, distinguishing cause from consequence in AD pathology remains challenging. Nevertheless, a notable observation is the early and progressive decline in constitutive proteasome subunit transcripts at initial Braak stages, preceding overt tau aggregation and neurofibrillary tangle formation. This suggests proteasome dysfunction may be an early event that predisposes neurons to subsequent protein aggregation and injury, aligning with previous studies showing progressive proteasome activity reductions in advancing Braak stages[20].

As proteotoxic stress escalates, transcriptional suppression becomes increasingly pronounced, potentially creating a detrimental feedback loop where decreased proteasome function promotes further protein aggregation. Our enzymatic assays confirm significantly impaired proteasome activity in AD brains. Crucially, proteasomes isolated from AD brains exhibit intrinsic defects even after purification, suggesting structural or compositional alterations within the complexes themselves, independent of external cellular factors.

Quantitative proteomics further highlights widespread disruption in proteostasis networks. Constitutive proteasome subunits and proteasome assembly chaperones are markedly reduced in neuron-rich grey matter regions severely impacted by AD pathology. Concurrently, aggregation-prone substrates, including tau, α-synuclein, and p62, accumulate alongside proteasomes,

potentially forming a "fibrous blanket" that inhibits substrate accessibility and exacerbates catalytic impairment. White matter displays more moderate changes, with preserved proteasome subunit abundance, aligning with snRNA-seq data revealing that non-neuronal cells maintain or even adapt their proteostatic machinery more effectively than neurons. Thus, neurons experience accelerated proteolytic capacity loss, corresponding to early transcriptional deficits, creating a permissive environment for disease progression.

A critical unresolved question is why intrinsic compensatory pathways fail to reverse early proteasome deficits. Normally, reduced proteasome activity stabilizes Nrf1 (NFE2L1), a transcription factor that translocates to the nucleus, driving proteasome gene expression, a mechanism termed the "bounce-back" response. Our ChIP-seq analyses confirm that NFE2L1 preferentially binds to proteasome gene promoters, and increased NFE2L1 transcripts suggest attempted compensation during AD progression. However, we observed that Nrf1 protein accumulates in the cytosol rather than translocating effectively into the nucleus in AD brains, thereby failing to restore proteasome gene expression. This uncoupling between elevated Nrf1 expression and inadequate transcriptional activation points to disrupted signaling in the bounce-back pathway.

Collectively, our data indicate that early transcriptional downregulation of proteasome genes, diminished proteolytic activity, and impaired Nrf1 signaling cumulatively compromise neuronal proteostasis. Rather than adaptively enhancing proteasome capacity in response to emerging proteotoxic stress, neurons in AD become trapped in a deleterious cycle of diminished proteasome availability and escalating protein aggregation. Thus, proteostasis dysfunction is not merely downstream of tau and amyloid pathology but represents a potential upstream driver, rendering neurons susceptible to protein accumulation. Therapeutically, our findings advocate for early interventions targeting proteasome function or Nrf1 signaling to preserve neuronal integrity and potentially mitigate AD progression.

Data availability

All data supporting the findings of this study are provided within the main text and supplementary materials, including figures and corresponding Excel files. Datasets from bulk

RNA-seq and snRNA-seq are available from AD Knowledge Portal: https://www.synapse.org/Synapse:syn2580853/wiki/409840, and NFE2L1 ChIP-seq data is available from ENCODE: https://www.encodeproject.org/experiments/ENCSR543SBE/.

Acknowledgements

We thank Dr. Marc Diamond for providing us with the HEK-293 RD-YFP (DS1 and DS9 clone) cell lines. We thank the Columbia University Alzheimer's Disease Research Center (ADRC), funded by NIH grant P30AG066462 to S.A. Small (P.I.) for providing recourses for the study. We thank Dr. Andrew Teich, the Director of The New York Brain Bank (NYBB) at Columbia University, for providing us with postmortem brains.

Funding

This work was funded by the NIA R01AG070075 and R01AG064244, awarded to N.M.

Competing interests

The authors report no competing interests.

Supplementary material

Supplementary material is available at *Brain* online.

References

1. De Strooper, B. & Karran, E. The Cellular Phase of Alzheimer's Disease. *Cell* **164**, 603-615 (2016).
2. Cole, G.M. & Timiras, P.S. Ubiquitin-protein conjugates in Alzheimer's lesions. *Neurosci Lett* **79**, 207-212 (1987).
3. Ciechanover, A. Proteolysis: from the lysosome to ubiquitin and the proteasome. *Nat Rev Mol Cell Biol* **6**, 79-87 (2005).
4. Finley, D., Ulrich, H.D., Sommer, T. & Kaiser, P. The ubiquitin-proteasome system of Saccharomyces cerevisiae. *Genetics* **192**, 319-360 (2012).
5. Collins, G.A. & Goldberg, A.L. The Logic of the 26S Proteasome. *Cell* **169**, 792-806 (2017).
6. Lander, G.C.*, et al.* Complete subunit architecture of the proteasome regulatory particle. *Nature* **482**, 186-191 (2012).
7. Chandran, A., Oliver, H.J. & Rochet, J.C. Role of NFE2L1 in the Regulation of Proteostasis: Implications for Aging and Neurodegenerative Diseases. *Biology (Basel)* **12**(2023).
8. Radhakrishnan, S.K.*, et al.* Transcription factor Nrf1 mediates the proteasome recovery pathway after proteasome inhibition in mammalian cells. *Mol Cell* **38**, 17-28 (2010).
9. Steffen, J., Seeger, M., Koch, A. & Kruger, E. Proteasomal degradation is transcriptionally controlled by TCF11 via an ERAD-dependent feedback loop. *Mol Cell* **40**, 147-158 (2010).
10. Sha, Z. & Goldberg, A.L. Proteasome-mediated processing of Nrf1 is essential for coordinate induction of all proteasome subunits and p97. *Curr Biol* **24**, 1573-1583 (2014).
11. Northrop, A., Byers, H.A. & Radhakrishnan, S.K. Regulation of NRF1, a master transcription factor of proteasome genes: implications for cancer and neurodegeneration. *Mol Biol Cell* **31**, 2158-2163 (2020).

12. Radhakrishnan, S.K., den Besten, W. & Deshaies, R.J. p97-dependent retrotranslocation and proteolytic processing govern formation of active Nrf1 upon proteasome inhibition. *Elife* **3**, e01856 (2014).

13. Myeku, N.*, et al.* Tau-driven 26S proteasome impairment and cognitive dysfunction can be prevented early in disease by activating cAMP-PKA signaling. *Nature medicine* **22**, 46-53 (2016).

14. Myeku, N. & Duff, K.E. Targeting the 26S Proteasome To Protect Against Proteotoxic Diseases. *Trends Mol Med* **24**, 18-29 (2018).

15. Schaler, A.W.*, et al.* PAC1 receptor-mediated clearance of tau in postsynaptic compartments attenuates tau pathology in mouse brain. *Sci Transl Med* **13**(2021).

16. Schaler, A.W. & Myeku, N. Cilostazol, a phosphodiesterase 3 inhibitor, activates proteasome-mediated proteolysis and attenuates tauopathy and cognitive decline. *Transl Res* **193**, 31-41 (2018).

17. Thibaudeau, T.A., Anderson, R.T. & Smith, D.M. A common mechanism of proteasome impairment by neurodegenerative disease-associated oligomers. *Nature communications* **9**, 1097 (2018).

18. Sudarsanareddy Lokireddy, N.V.K., Alfred L. Goldberg. cAMP-induced phosphorylation of 26S proteasomes on Rpn6/PSMD11 enhances their activity and the degradation of misfolded proteins. *Proc. Natl. Acad. Sci* (2015).

19. VerPlank, J.J.S., Tyrkalska, S.D., Fleming, A., Rubinsztein, D.C. & Goldberg, A.L. cGMP via PKG activates 26S proteasomes and enhances degradation of proteins, including ones that cause neurodegenerative diseases. *Proceedings of the National Academy of Sciences of the United States of America* **117**, 14220-14230 (2020).

20. Chocron, E.S.*, et al.* Genetic and pharmacologic proteasome augmentation ameliorates Alzheimer's-like pathology in mouse and fly APP overexpression models. *Science advances* **8**, eabk2252 (2022).

21. Ribeiro, F.C.*, et al.* Synaptic proteasome is inhibited in Alzheimer's disease models and associates with memory impairment in mice. *Communications biology* **6**, 1127 (2023).

22. Minis, A., *et al.* The proteasome regulator PI31 is required for protein homeostasis, synapse maintenance, and neuronal survival in mice. *Proceedings of the National Academy of Sciences of the United States of America* **116**, 24639-24650 (2019).

23. Ferrington, D.A. & Gregerson, D.S. Immunoproteasomes: structure, function, and antigen presentation. *Progress in molecular biology and translational science* **109**, 75-112 (2012).

24. Basler, M., Kirk, C.J. & Groettrup, M. The immunoproteasome in antigen processing and other immunological functions. *Curr Opin Immunol* **25**, 74-80 (2013).

25. Heneka, M.T., Golenbock, D.T. & Latz, E. Innate immunity in Alzheimer's disease. *Nat Immunol* **16**, 229-236 (2015).

26. Sanders, D.W., *et al.* Distinct tau prion strains propagate in cells and mice and define different tauopathies. *Neuron* **82**, 1271-1288 (2014).

27. Hipp, M.S., Kasturi, P. & Hartl, F.U. The proteostasis network and its decline in ageing. *Nat Rev Mol Cell Biol* **20**, 421-435 (2019).

28. Soto, C. & Pritzkow, S. Protein misfolding, aggregation, and conformational strains in neurodegenerative diseases. *Nat Neurosci* **21**, 1332-1340 (2018).

29. Keller, J.N., Hanni, K.B. & Markesbery, W.R. Impaired proteasome function in Alzheimer's disease. *Journal of neurochemistry* **75**, 436-439 (2000).

30. Keck, S., Nitsch, R., Grune, T. & Ullrich, O. Proteasome inhibition by paired helical filament-tau in brains of patients with Alzheimer's disease. *Journal of neurochemistry* **85**, 115-122 (2003).

31. Braak, H. & Braak, E. Neuropathological stageing of Alzheimer-related changes. *Acta Neuropathol* **82**, 239-259 (1991).

32. De Jager, P.L., *et al.* A multi-omic atlas of the human frontal cortex for aging and Alzheimer's disease research. *Sci Data* **5**, 180142 (2018).

33. Sjobeck, M. & Englund, E. Glial levels determine severity of white matter disease in Alzheimer's disease: a neuropathological study of glial changes. *Neuropathol Appl Neurobiol* **29**, 159-169 (2003).

34. Besche, H.C. & Goldberg, A.L. Affinity purification of mammalian 26S proteasomes using an ubiquitin-like domain. *Methods Mol Biol* **832**, 423-432 (2012).

35. Myeku, N., Metcalfe, M.J., Huang, Q. & Figueiredo-Pereira, M. Assessment of proteasome impairment and accumulation/aggregation of ubiquitinated proteins in neuronal cultures. *Methods Mol Biol* **793**, 273-296 (2011).

36. Tomko, R.J., Jr. & Hochstrasser, M. Molecular architecture and assembly of the eukaryotic proteasome. *Annu Rev Biochem* **82**, 415-445 (2013).

37. Wang, M.*, et al.* The Mount Sinai cohort of large-scale genomic, transcriptomic and proteomic data in Alzheimer's disease. *Sci Data* **5**, 180185 (2018).

38. Allen, M.*, et al.* Human whole genome genotype and transcriptome data for Alzheimer's and other neurodegenerative diseases. *Sci Data* **3**, 160089 (2016).

39. Orre, M.*, et al.* Reactive glia show increased immunoproteasome activity in Alzheimer's disease. *Brain : a journal of neurology* **136**, 1415-1431 (2013).

40. Fujita, M.*, et al.* Cell subtype-specific effects of genetic variation in the Alzheimer's disease brain. *Nat Genet* **56**, 605-614 (2024).

41. Mathys, H.*, et al.* Single-cell multiregion dissection of Alzheimer's disease. *Nature* **632**, 858-868 (2024).

42. Hsieh, Y.C.*, et al.* Person-specific differences in ubiquitin-proteasome mediated proteostasis in human neurons. *Alzheimer's & dementia : the journal of the Alzheimer's Association* **20**, 2952-2967 (2024).

43. Consortium, E.P. An integrated encyclopedia of DNA elements in the human genome. *Nature* **489**, 57-74 (2012).

44. Pickering, A.M., Linder, R.A., Zhang, H., Forman, H.J. & Davies, K.J.A. Nrf2-dependent induction of proteasome and Pa28alphabeta regulator are required for adaptation to oxidative stress. *The Journal of biological chemistry* **287**, 10021-10031 (2012).

45. Tonoki, A.*, et al.* Genetic evidence linking age-dependent attenuation of the 26S proteasome with the aging process. *Mol Cell Biol* **29**, 1095-1106 (2009).

Figure legends

Figure 1 Reduced proteolytic capacity of proteasomes in AD brains. (**A–D**) Kinetic analyses of proteasome activity in total lysates isolated from (**A,B**) grey and (**C,D**) white matter. Proteasome activity was measured using the fluorogenic substrate Suc-LLVY–amc, and the rate of substrate hydrolysis was monitored over 120 minutes. (**A,C**) Representative kinetic curves of substrate hydrolysis in control (blue) and AD (pink) samples. (**B,D**) Quantification of the average proteasome activity as a percentage of control levels after two hours. Proteasome-mediated proteolysis is significantly decreased in both grey and white matter in AD. (Control n = 20, AD n = 26. Control: blue circles; AD: pink circles). (**E–H**) Kinetic analyses of purified 26S proteasomes from (**E,F**) grey and (**G,H**) white matter (control n = 9, AD n = 9). Similar to total lysates, purified proteasomes from AD brains show a marked reduction in substrate hydrolysis rate. (**E,G**) Representative kinetic curves. (**F,H**) Quantification of proteasome activity expressed as a percentage of control confirms a significant intrinsic impairment of proteolytic capacity in AD-derived proteasomes. (**I–L**) Native in-gel proteasome activity assays. (**I,K**) Representative non-denaturing gels incubated with Suc-LLVY–amc substrate to visualize 26S and 20S proteasome activity in (**I**) grey and (**K**) white matter (control n = 6, AD n = 12). Lower panels show corresponding actin immunoblots as loading controls. (**J,L**) Quantification of proteasome activity bands expressed as a percentage of control. In (**J**) grey matter, both 26S and 20S activities are significantly reduced in AD. In (**L**) white matter only 26S activity is significantly diminished in AD, while 20S activity is not significantly affected. Each point represents an individual non-overlapping sample (control n = 35, AD n = 47) (control: blue circles; AD: pink circles). All data are presented as mean ± SEM. ns = non-significant, *p<0.05, **p<0.01, ***p<0.001, ****p<0.0001; unpaired t-tests.

Figure 2 Proteomic and network analyses of gel-isolated 26S proteasomes in AD. (**A,B**) Volcano plots showing differentially abundant proteins from gel-isolated 26S proteasomes from the grey matter of AD versus control brains (control n = 12, AD n = 14). Each point represents a protein, with the x-axis indicating log2 (fold change) and the y-axis indicating –log10(p-value). The dashed vertical and horizontal lines denote significance thresholds. (**A**) Overall proteomic changes reveal numerous proteins decreased (blue) and increased (red) in AD. (**B**) Focusing on

proteasome subunits and related factors, a pronounced reduction in constitutive proteasome components is observed in AD grey matter. (**C**) Heatmap of selected UPS-related proteins, including E3 ubiquitin ligases, deubiquitinating enzymes (DUBs), molecular chaperones, and proteasome subunits (19S, 20S, immunoproteasome (IP), and assembly chaperones) in grey matter. Each column represents an individual sample, and each row corresponds to a protein. The color scale indicates relative abundance changes (Z-scores), with blue representing decreased abundance and red increased abundance in AD. Grey matter shows a marked downregulation of constitutive proteasome subunits and associated assembly factors. (**D**) Protein–protein interaction (PPI) network for differentially abundant UPS-related factors in grey matter. Red nodes indicate proteins increased in AD, and blue nodes indicate proteins decreased in AD. The center of the network is dominated by reduced proteasome subunits and stabilizing factors, reflecting a core proteostatic disruption in grey matter. Reduced (blue node) proteins that have functional or physical connections to the 26S proteasome: ADRM1 – 26S proteasome receptor (Rpn13). AMBRA1 – component of a CUL4-DDB1 E3-ligase complex. BAG3 – Hsp70 co-chaperone. CCT2 and CCT3– TRiC/CCT chaperonin subunit. COPS2 – COPS9 signalosomes regulating CRL E3 ligases. CUL1 and CUL3 – cullin scaffold of SCF/BTB-type E3 ubiquitin ligases. ECM29 – proteasome-anchoring protein that stabilizes 26S assemblies. HSP90AB1 – cytosolic Hsp90; HSPA4 – Hsp70 family chaperone. HSPA5 –ER chaperone coordinating ERAD. HSPA9 – mitochondrial Hsp70. HUWE1 – HECT-type E3 ubiquitin ligase. ISG15 – ubiquitin-like modifier. NEDD8 – ubiquitin-like modifier. PRPF19 – component of an E3 ligase complex (Prp19 complex). RUVBL1 – AAA+ ATPase complex. STIP1 – Hsp70/Hsp90 organizing protein. VCP (p97) – AAA-ATPase that extracts ubiquitinated clients for proteasomal degradation. Increased (red node) proteins that have functional or physical connections to the 26S proteasome: FAM175B (ABRO1) – scaffold of the BRISC de-ubiquitinase complex. HSPA1A (Hsp70-1) – chaperone. HSPA8 (Hsc70) – constitutive Hsp70. HSPD1 (Hsp60) – mitochondrial chaperone. NPLOC4 – adaptor for the VCP/p97. RAD23B – UbL-UBA shuttle factor. RPS27A (Ub-S27a) – poly-ubiquitin fusion protein. SKP1 – core subunit of SCF Cullin-1 E3 ligases. TRAP1 – mitochondrial Hsp90. UBC – free ubiquitin. UBLCP1 – nuclear proteasome phosphatase. UBQLN2 – UbL-UBA shuttle protein. USP14 – proteasome-associated de-ubiquitinase. MAPT - tau. SNCA -α-synuclein. (**E,F**) Volcano plots for gel-isolated 26S proteasomes from white matter (n = 6, AD n = 8), analogous to panels (A,B). While significant alterations occur, the changes in

proteasome subunits are less pronounced than in grey matter. Some proteins are decreased (blue) or increased (red), but constitutive proteasome components do not show as strong a depletion. (**G**) Heatmap of UPS-related proteins in white matter. Similar to (C), but the pattern is more subtle. Although some changes occur, the core proteasome subunits and assembly chaperones are not consistently downregulated, suggesting white matter proteostasis is less severely affected than grey matter. (**H**) PPI network of differentially abundant proteins in white matter. Although certain factors are altered, the network does not show the same profound depletion of proteasome subunits seen in grey matter. Reduced (blue node) proteins that have functional or physical connections to the 26S proteasome: CUL1, CUL3, CCT2 / CCT3, HSP90AB1, SNCA. Increased (red node) proteins that have a functional or physical connections to the 26S proteasome: ADRM1, COPS3, HSPA1A, HSPA4, HSPA8, HSPA9, HSPD1, STIP1, VCP/p97, UBA52 (Ub-L40 fusion), PRPF19 (PRP19/PSO4) – E3 ligase–spliceosome. Together, these analyses indicate that grey matter experiences a pronounced loss of proteasome complexes and broad destabilization of proteostasis networks in AD. In contrast, white matter remains relatively more stable, reflecting distinct region-specific vulnerabilities in the AD brain.

Figure 3 Proteomic and network analyses of affinity purified 26S proteasomes in AD. (**A,B**) Volcano plots illustrating changes in protein abundance in affinity-purified 26S proteasomes from grey matter in AD versus controls (control n = 10, AD n = 10). Each point represents an individual protein, with the x-axis showing log2 (fold change) and the y-axis displaying −log10(p-value). Dashed lines indicate significance thresholds. (**A**) Overall differentially abundant proteins are seen, with several proteins decreased (blue) or increased (red) in AD. (**B**) Focusing on proteasome subunits and related factors, a depletion of constitutive proteasome components is observed in AD grey matter even after proteasome purification. (**C**) Heatmap showing relative abundances (Z-scores) of selected UPS-related proteins in grey matter, including E3 ligases, deubiquitinating enzymes (DUBs), molecular chaperones, and proteasome subunits (19S, 20S, immunoproteasome (IP) components, and assembly factors). Each column is an individual sample, grouped by condition (Control vs. AD). The pronounced downregulation of proteasome subunits and assembly factors in AD is evident, consistent with impaired proteostasis in grey matter. (**D**) PPI network of differentially abundant UPS-related factors in grey matter. Red nodes represent proteins increased in AD, while blue nodes represent decreased proteins. The network's center is enriched for

downregulated proteasome subunits and associated factors, highlighting a core proteostatic defect in AD grey matter. Reduced (blue node) proteins that have functional or physical connections to the 26S proteasome. ADRM1, COPS2-6, CUL1, DDI2 – aspartyl protease that cleaves Nrf1 for transcriptional activity, ECM29, FAM175B (ABRAXAS-2) – component of the BRISC de-ubiquitinase complex that interacts with proteasomes, HUWE1, NPLOC4, TXNL1 – redox-sensitive proteasome-interacting protein that modulates 20S gate opening, UBC, UBE3A (E6-AP) – HECT-domain E3 ubiquitin ligase implicated in synaptic proteostasis, UBL7 – ubiquitin-like protein, UBQLN1, UBQLN2, UBXN1 – UBX-domain p97 adaptor, USP14, VCP/p97, CCT2, CCT3. Increased (red node) proteins that have functional or physical connections to the 26S proteasome: MAPT, SQSTM1/p62, SNCA, HSPA1A, HSPA4, HSPA9, HSPD, STIP1, RAD23B, CUL3, SKP1. (**E,F**) Volcano plots of affinity purified 26S proteasome from white matter from AD and control samples (control n = 10, AD n = 9), similar to (A,B). Although some proteins are significantly altered, the depletion of proteasome components is less pronounced than in grey matter. White matter shows more subtle changes, indicating comparatively better maintenance of proteostasis. (**G**) Heatmap of UPS-related proteins in white matter, analogous to (**C**). While some components are altered, the pattern is less severe than in grey matter. Core proteasome subunits and chaperones are not uniformly downregulated, suggesting that proteostasis in white matter remains relatively intact or better compensated. (**H**) PPI network of differentially abundant proteins of purified proteasomes in white matter similar to (**D**). Reduced (blue node) proteins that have functional or physical connections to the 26S proteasome. VCP / p97, USP14, UBQLN2, HSP90AB1, HSPA9, STIP1, CCT2, CCT3, SNCA, RAC1, UBE3A (E6-AP). Increased (red node) proteins that have functional or physical connections to the 26S proteasome: ADRM1, COPS2-COPS6, CUL1, CUL3, HUWE1, RAD23B, SKP1, MAPT, HSPA1A, HSPA4, HSPA5, HSPA8, HSPD1. Although alterations occur, the network does not reveal a profound depletion of proteasome subunits. This balanced scenario implies that white matter is less vulnerable to proteostasis collapse than grey matter. Overall, these data demonstrate a more pronounced proteasome-related proteostasis deficit in AD grey matter, while white matter is relatively spared or better adapted, underscoring region-specific differences in how AD pathology affects protein quality control systems.

Figure 4 Progressive downregulation of constitutive proteasome subunits and differential responses of immunoproteasome across multiple AD cohorts. (**A–C**) Heatmaps showing the normalized expression (Z-scores) of constitutive proteasome subunits, assembly chaperones, and immunoproteasome (IP) components across increasing Braak stages for three independent cohorts of bulk-RNAseq datasets: (**A**) MSBB, (**B**) ROSMAP, and (**C**) Mayo Clinic Study of Aging. Each column represents a sample ordered by Braak stage (0-VI), while rows depict individual proteasome-related genes. Warmer colors (reds) indicate higher relative expression, and cooler colors (blues) indicate lower expression. A clear trend emerges where constitutive proteasome subunits (19S and 20S) and assembly chaperones decline with the advancing Braak stage, whereas immunoproteasome subunits show less consistent changes. (**D–F**) Boxplots of Z-scores for aggregated proteasome complexes and factors, 19S, 20S, assembly chaperones, immunoproteasome (IP), and IP activator complexes—grouped by Braak stage in (**D**) MSBB, (**E**) ROSMAP, and (**F**) Mayo cohorts. Each colored point or bar corresponds to a specific Braak stage. As Braak stage increases, 19S and 20S components consistently show a downward trend, while immunoproteasome and IP activator complexes remain relatively stable or exhibit compensatory changes. (**G**) Meta-analysis combining results from MSBB, ROSMAP, and Mayo cohorts. Forest plots present standardized mean differences across studies for key proteasome-related groups (19S, 20S, IP activator, immunoproteasome, and assembly chaperones). Negative values indicate reduced abundance in AD relative to controls. The meta-analysis confirms a robust, consistent decrease in constitutive proteasome subunits and assembly chaperones, while immunoproteasome components show more variable or modest changes. Together, these data demonstrate a reproducible and progressive loss of constitutive proteasome capacity across multiple cohorts and brain regions. The early and sustained downregulation of 19S and 20S proteasome components with AD pathology suggests a fundamental disruption in neuronal proteostasis, potentially contributing to the accumulation of aggregation-prone proteins as the disease advances.

Figure 5 Cell-type–specific changes in proteasome-related gene expression across AD progression, as revealed by snRNA-seq datasets. (**A,B**) Circular heatmaps illustrating the Z-scored expression patterns of proteasome subunits, assembly chaperones, immunoproteasome (IP) components, and IP activator complexes across increasing Braak stages in distinct brain cell types. Each concentric ring represents a Braak stage, and each radial segment corresponds to a

proteasome complex class (e.g., 19S, 20S, assembly chaperones, IP, IP activator complexes), while each wedge of the circle denotes a specific cell type. Warmer colors (reds) indicate higher relative expression, and cooler colors (blues) indicate lower relative expression. Braak stages increase outward from the center. (**A**) Data from Fujita et al.[40] show that excitatory (Ex) and inhibitory (In) neurons progressively lose expression of constitutive proteasome subunits and assembly chaperones as Braak stage advances, shifting from red to blue hues. In contrast, non-neuronal cells (e.g., astrocytes (Ast), microglia (Mic), oligodendrocyte lineage (Oli), oligodendrocyte precursor cells (Opc), and endothelial cells (End)) maintain or even increase certain proteasome-related transcripts, indicating a more resilient or compensatory response. (**B**) Data from Mathys et al.[41] similarly confirm a neuron-specific decline in constitutive proteasome gene expression with advancing Braak stages. Non-neuronal cell types again show relatively stable or less severely impacted proteasome-related expression patterns, consistent with the findings from Fujita et al. Together, these snRNA-seq data from two independent datasets underscore a fundamental, cell-type–dependent vulnerability in AD, with neurons showing pronounced proteasome gene downregulation as disease pathology escalates, while non-neuronal cells retain or bolster their proteostasis capacity.

Figure 6 NFE2L1 preferential binding to proteasome genes but exhibits ineffective proteasome recovery in advanced AD. (**A**) Density plots of NFE2L1 ChIP-seq signal distributions for proteasome-related genes (blue) versus a background set of randomly selected genes (pink). Each curve represents the probability density of mean NFE2L1 ChIP-seq values obtained via random sampling. The vertical dashed lines indicate the median signal values for background (pink line) and proteasome (blue line) gene sets. The clear shift in the distribution toward higher values for proteasome genes, supported by a significant p-value ($P = 9.814 \times 10^{-4}$), indicates that NFE2L1 preferentially occupies proteasome gene promoters relative to random genomic loci. This enrichment highlights NFE2L1's key regulatory role in driving proteasome gene transcription under proteostatic stress conditions. (**B**) Transcriptional changes in NFE2L1 and NFE2L2 relative to Braak stage from the three bulk RNAseq datasets (MSBB, ROSMAP and Mayo). Normalized expression data reveal that NFE2L1 and NFE2L2 transcripts increase at later Braak stages, despite declining proteasome gene expression. **(C)** The "NFE2L1 resist score" (difference between predicted vs. observed proteasome abundance based on NFE2L1 transcripts)

grows more positive as Braak stage advances, indicating that elevated NFE2L1 expression does not translate into restored proteasome function ($p=9.88\times10^{-7}$). Although NFE2L1 preferentially occupies proteasome gene promoters and both NFE2L1/NFE2L2 transcripts increase at later Braak stages, these elevations fail to restore proteasome expression and function. The growing "NFE2L1 resist score" and cell-type–resolved data suggest that, despite heightened transcription factor presence, neurons cannot effectively upregulate proteasome genes as AD pathology advances. This disconnect highlights a critical failure in the compensatory mechanism intended to maintain proteostasis, contributing to the progression of Alzheimer's disease.

Figure 7 Impaired Nrf1 nuclear translocation in AD and an impaired bounce-back response of proteasomes. (**A–D**) Western blot analysis of Nrf1, PSMG1 and Rpt5/PSMC3 in proteasome-enriched soluble cortical extracts from control and AD brains (control n = 9, AD n = 9). (**A**) Representative immunoblots. Actin serves as a loading control. (**B–D**) Quantifications show that (**B**) total Nrf1 levels are significantly elevated in AD, while (**C**) PSMG1 is markedly reduced and (**D**) Rpt5/PSMC3 levels are not significantly reduced. (**E–G**) Subcellular fractionation of cortical extracts to assess Nrf1 localization. (**E**) Representative blots of total, cytosolic, and nuclear fractions from control and AD brains (control n = 15, AD n = 15). Lamin A/C and GAPDH are used as nuclear and cytosolic markers, respectively, and actin as a loading control. (**F,G**) Quantifications of upper and lower Nrf1 bands (corresponding to different post-translationally modified forms) show that total Nrf1 levels were unchanged between groups whereas the cytosolic levels were increased in AD. Contrary to the cytosolic Nrf1, nuclear Nrf1 is significantly decreased in AD. This suggests impaired nuclear translocation or processing of Nrf1 required for effective transcriptional activation of proteasome genes. **(H)** Representative Western blots showing Nrf1, PSMG1 and Rpt5 in total lysates, cytosolic, and nuclear fractions of two cell lines (DS1 and DS9) treated with or without epoxomicin, a proteasome inhibitor (four biological experiments). Lamin A/C serves as a nuclear marker, GAPDH as a cytosolic marker, and β-actin as a loading control. **(B–D)** Quantifications of (**B**) Nrf1, (**C**) PSMG1, and (**D**) Rpt5 levels comparing DS9 to DS1, a control condition. In the absence of epoxomicin, Nrf1 (upper and lower bands) undergoes rapid degradation, maintaining low basal levels (DS1cells, control condition). Upon reduced proteasome activity under persistent tau aggregation (DS9 cells condition) Nrf1 upper and lower bands increase in all the fractions. Upon proteasome inhibition with epoxomicin, cytosolic Nrf1

accumulates in the nucleus, indicative of the activated "bounce-back" response aimed at restoring proteasome capacity. This response includes upregulation of PSMG1 in both total and nuclear fractions. Rpt5 levels also show modest changes. These results demonstrate that pharmacological proteasome inhibition can recapitulate aspects of the compensatory mechanism attempting to restore proteasome homeostasis and highlight the enhanced responsiveness in a proteostasis-compromised cell line (DS9). Data are presented as mean ± SEM; each point represents an individual sample; ns = not significant, *p<0.05, **p<0.01, ***p<0.001.

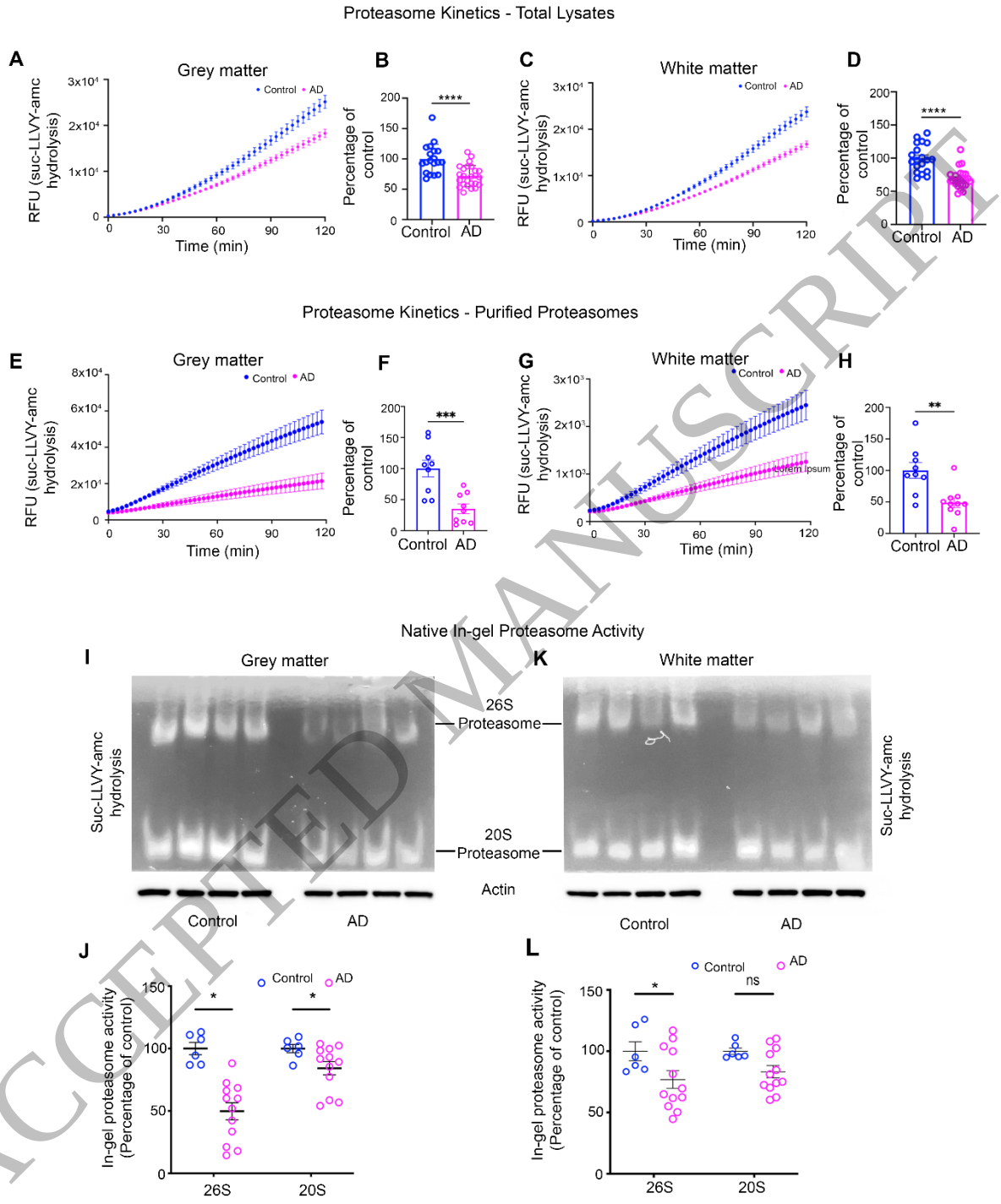

Figure 1
159x194 mm (x DPI)

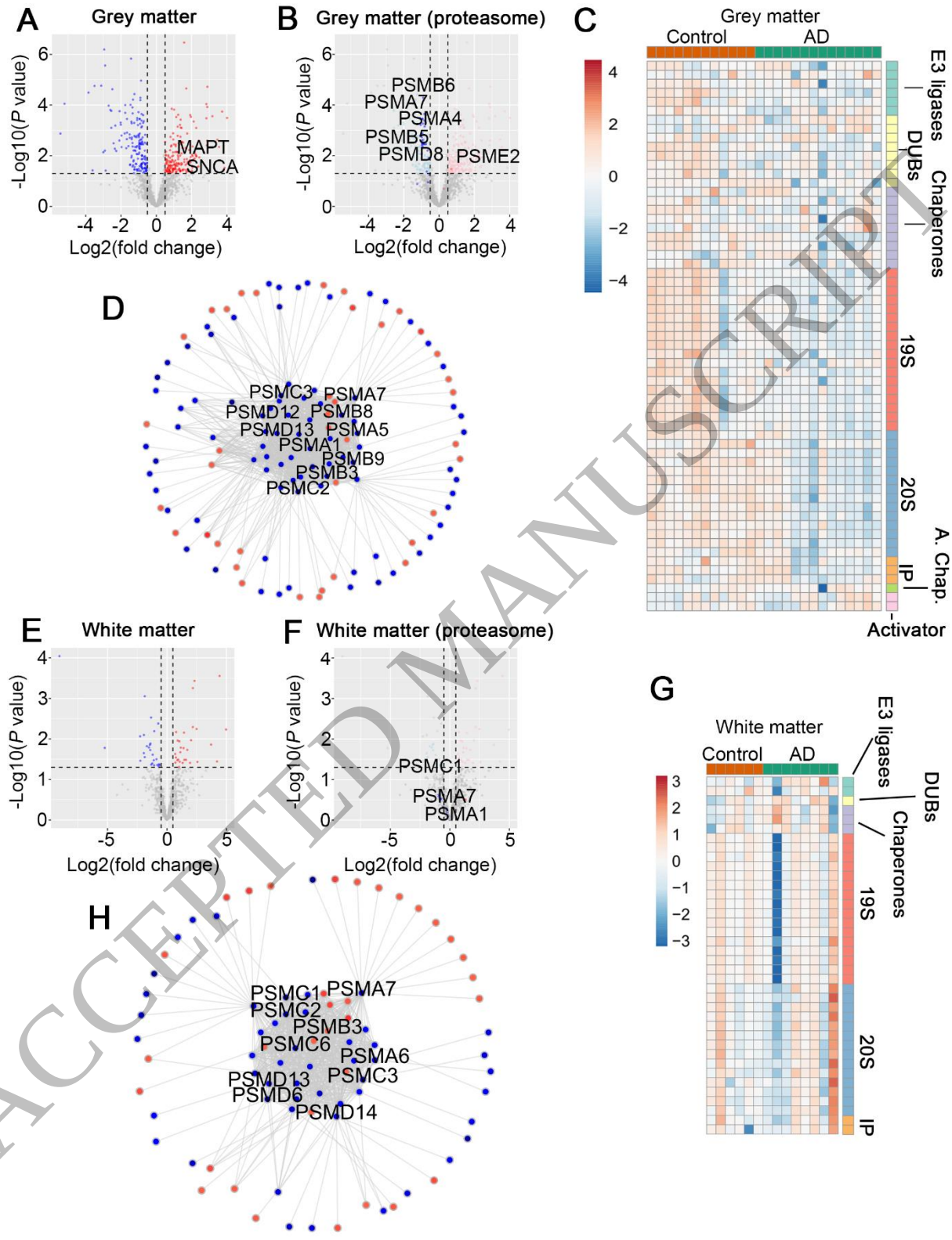

Figure 2
159x209 mm (x DPI)

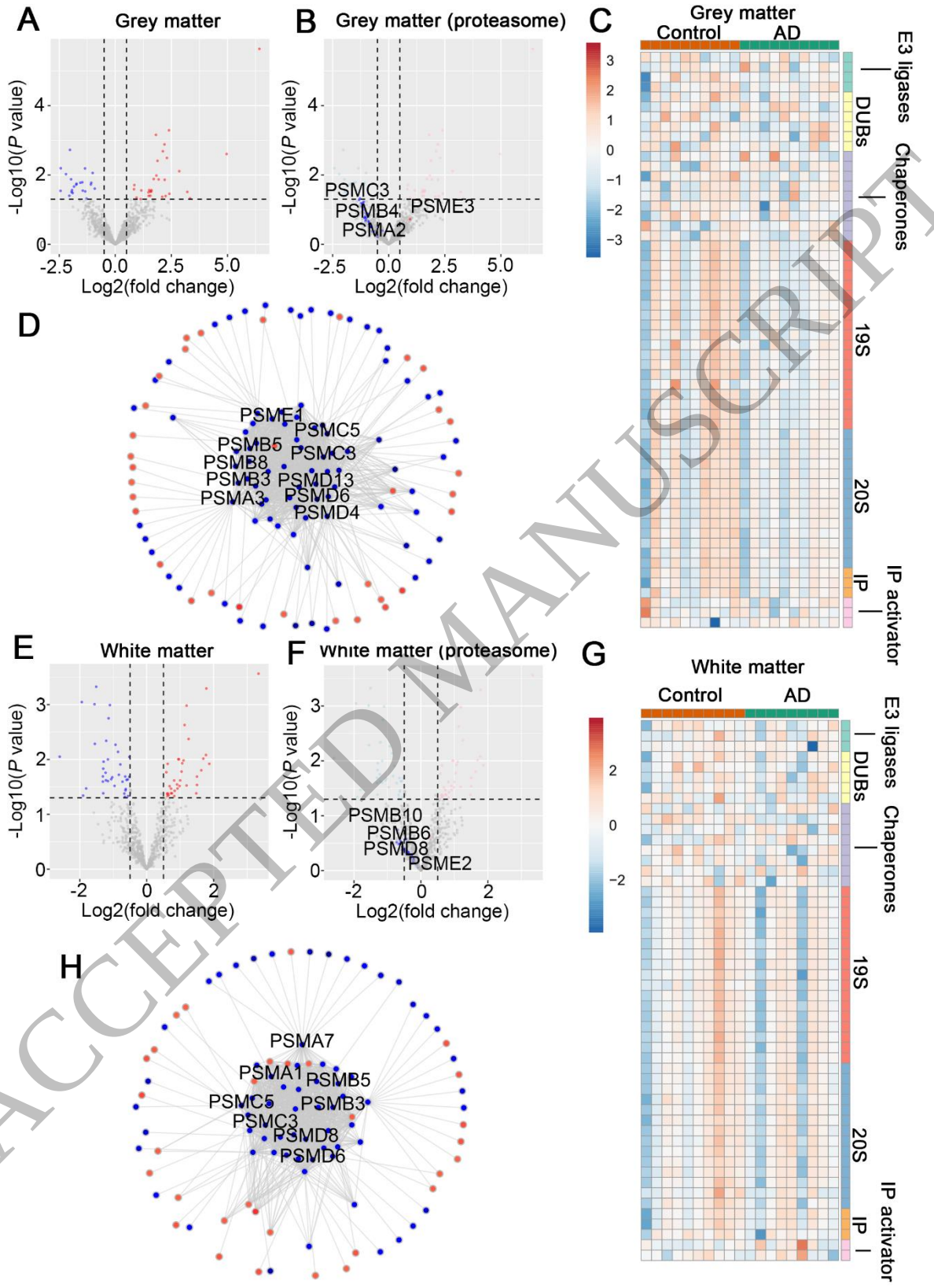

Figure 3
159x217 mm (x DPI)

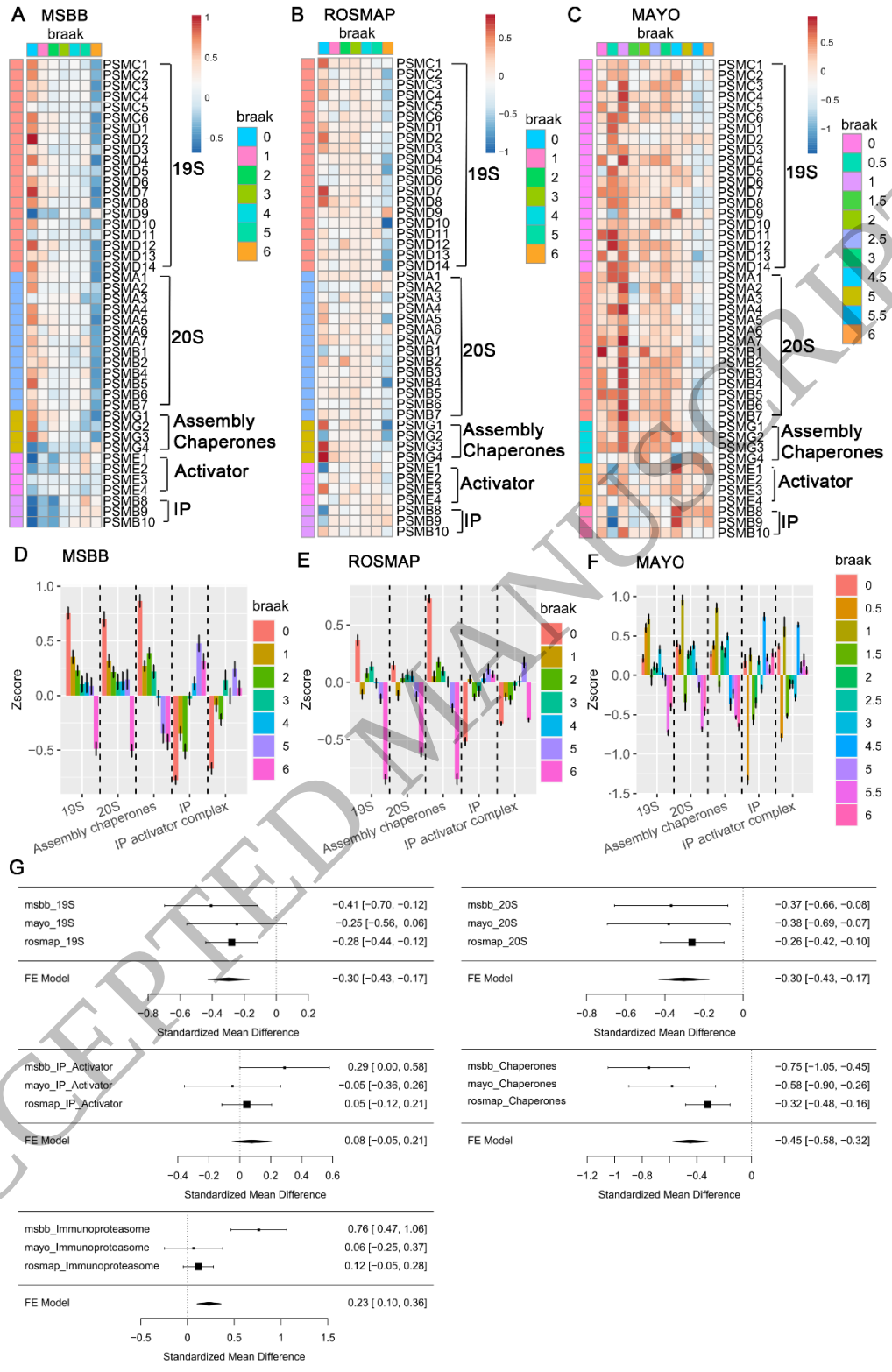

Figure 4
159x246 mm (x DPI)

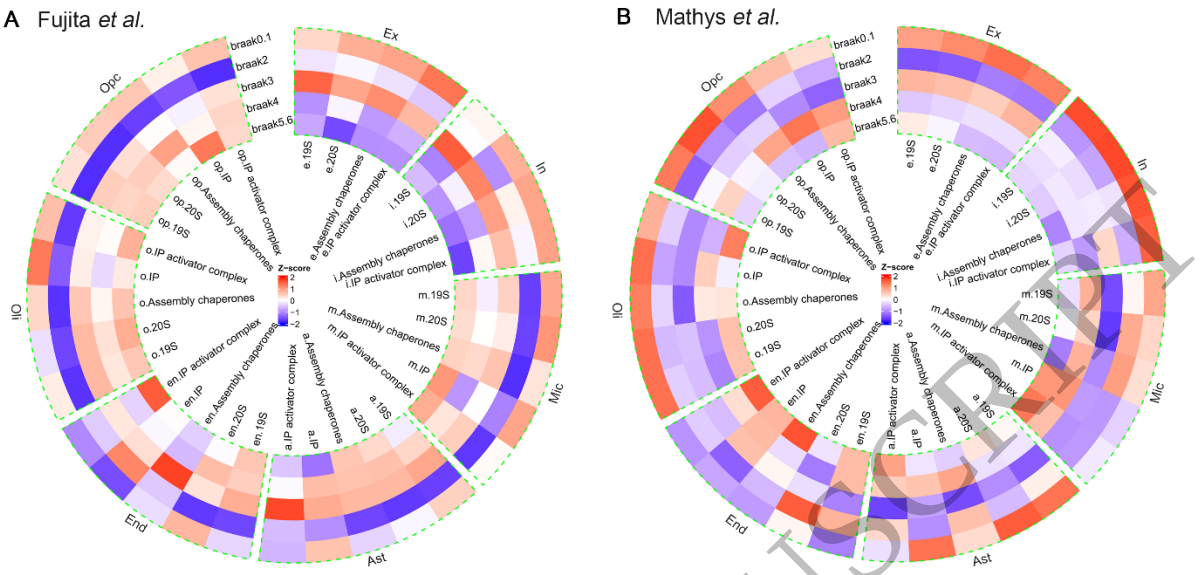

Figure 5
159x80 mm (x DPI)

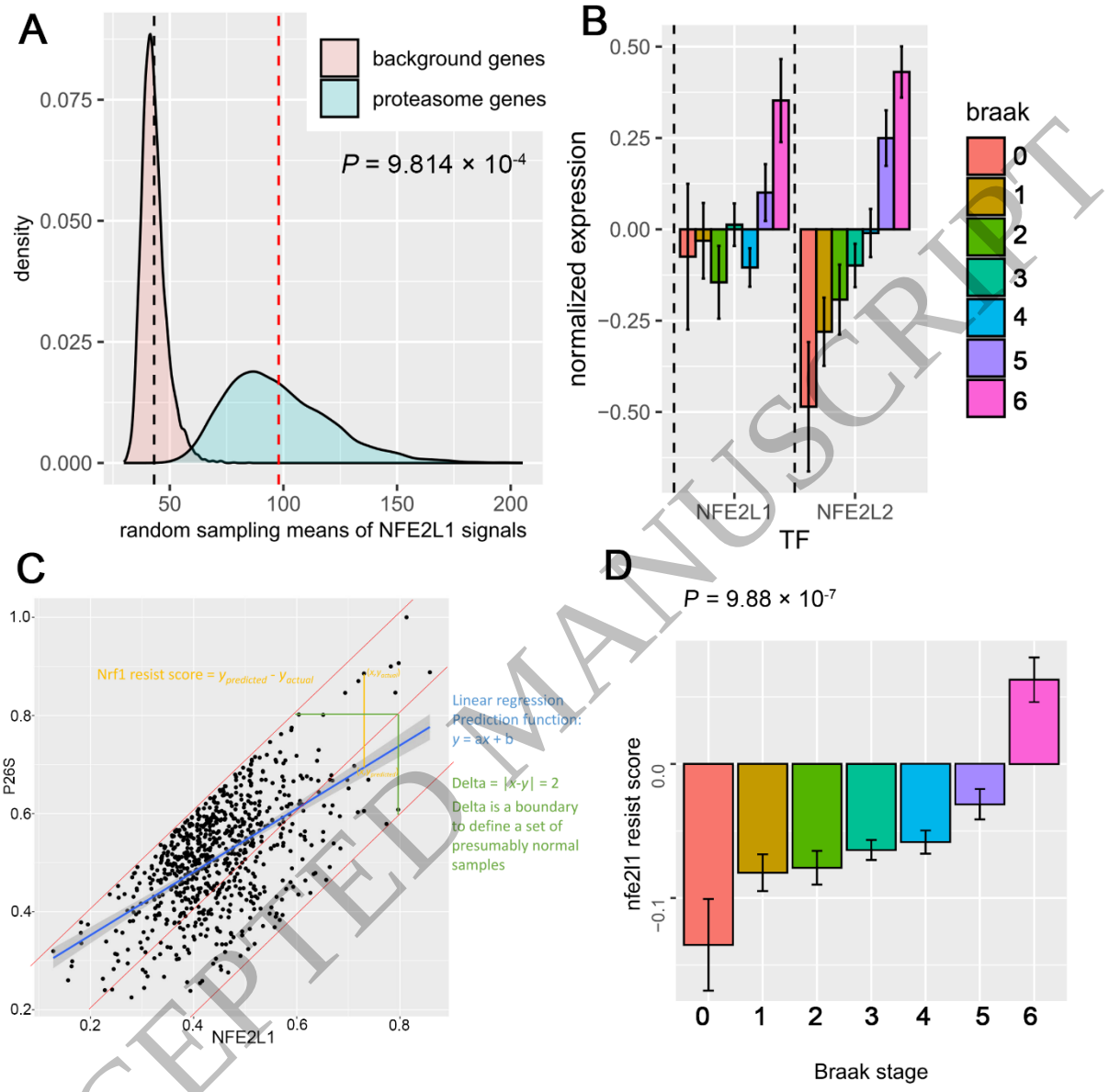

Figure 6
159x165 mm (x DPI)

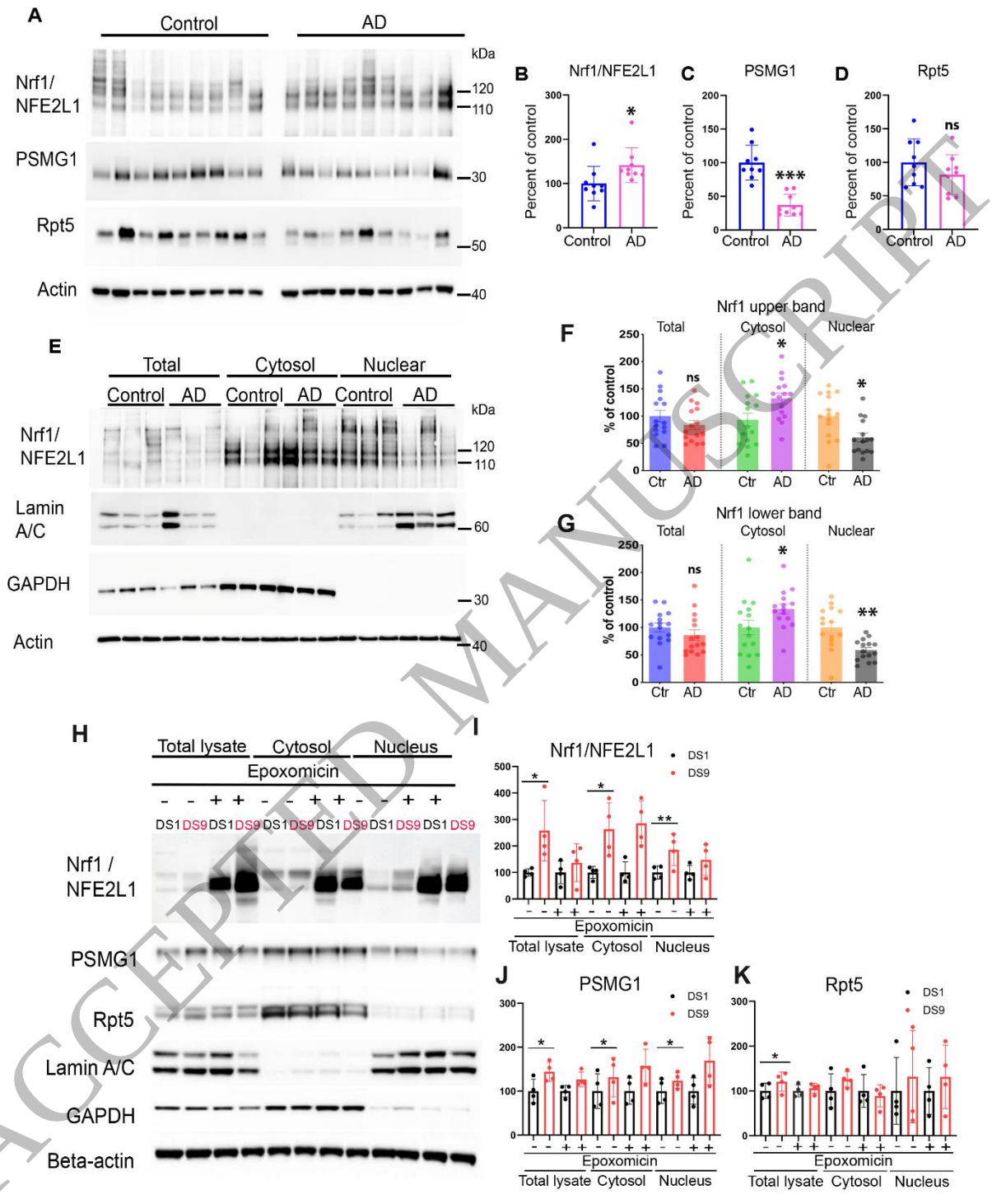

Figure 7
159x196 mm (x DPI)